RESEARCH ARTICLE SUMMARY

LINEAGE TRACING

Proliferation tracing reveals regional hepatocyte generation in liver homeostasis and repair

Lingjuan He*, Wenjuan Pu*, Xiuxiu Liu*, Zhenqian Zhang, Maoying Han, Yi Li, Xiuzhen Huang, Ximeng Han, Yan Li, Kuo Liu, Mengyang Shi, Liang Lai, Ruilin Sun, Qing-Dong Wang, Yong Ji, Jan S. Tchorz, Bin Zhou†

INTRODUCTION: Cell proliferation is a fundamental process in all multicellular organisms that is required to enable development, tissue homeostasis, tissue repair, and tissue regeneration. Disrupted proliferation is the pathogenic basis of many diseases. The ability to monitor cell proliferation has been essential for a myriad of studies in developmental biology, oncology, immunology, neuroscience, and regenerative medicine. The limitations of current approaches for measuring cell proliferation in vivo have left many fundamental questions in numerous life science fields insufficiently addressed. For example, decades of research have resulted in a controversial debate around zonal hepatocyte proliferation in liver homeostasis, repair, and regeneration.

RATIONALE: To provide a high–spatiotemporal resolution examination of in vivo cell proliferation, we take advantage of two orthogonal, site-specific recombinases (Cre and Dre) to develop a genetic proliferation lineage tracing method—proliferation tracer (ProTracer). ProTracer enables the temporally continuous recording of cell proliferation events with high spatial resolution in specific cell lineages. Highlighting its capabilities, we provide insights into the regional proliferation of adult mouse hepatocytes, which are heterogeneous in gene expression and function. Previous conflicting studies identifying hepatocytes with superior proliferative capacity have mostly relied on the lineage tracing of a subset of cell populations, thereby introducing a potential selective bias. Whether a specific population of hepatocytes with increased proliferative capacity exists remains unclear. Rather than tracing only a subset of the whole hepatocyte population, an unbiased assessment of proliferative events in the entire hepatocyte pool over time is needed to address this fundamental question.

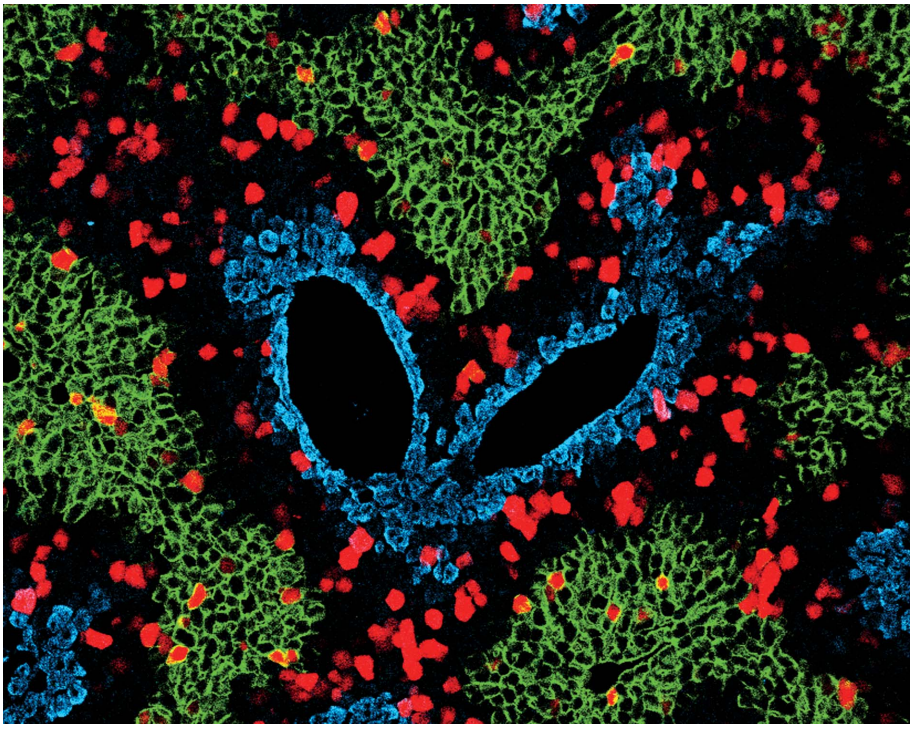

Highly regional hepatocyte generation in adult liver during tissue homeostasis. Immunostaining for E-cadherin (E-CAD) (green), glutamine synthetase (GS) (blue), and tdTomato (red; ProTracer signal) on liver sections of hepatocyte-specific ProTracer mice. Hepatocyte proliferation events ($tdTomato^+$) genetically recorded by ProTracer are highly enriched in the $E\text{-}CAD^-GS^-$ midlobular zone during liver homeostasis.

RESULTS: After an initial pulse treatment of tamoxifen, ProTracer permits the temporally continuous genetic recording of in vivo cell proliferation in diverse cell lineages over time in multiple organs and tissues. Using a hepatocyte-specific promoter, ProTracer could be primed to specifically record proliferation in hepatocytes—and not any other cell lineages—in the mouse liver. Furthermore, ProTracer enables noninvasive, long-term monitoring of hepatocyte proliferation over time in live animals. Cell proliferation tracing revealed that, at the whole hepatocyte–population level, more proliferation was detected in a subset of midzonal hepatocytes during liver homeostasis, with less proliferation in periportal hepatocytes and minimal proliferation in pericentral hepatocytes. Clonal analysis showed that most of the hepatocytes labeled by ProTracer have undergone cell division. Additionally, a highly regional and dynamic hepatocyte generation pattern was observed during repair and regeneration in response to several liver injuries, such as partial hepatectomy, bile duct ligation, and carbon tetrachloride–induced liver injury. Furthermore, genetic tracing of the proliferation of other cell lineages by ProTracer revealed distinct cell proliferation dynamics of macrophages, biliary epithelial cells, endothelial cells, and hepatic stellate cells after partial hepatectomy.

CONCLUSION: Our work provides a genetic system for the cumulative recording of cell type–specific proliferation in vivo. By genetically tracing the proliferation events of entire cell populations, ProTracer enables the unbiased detection of the specific cell population that mainly accounts for tissue homeostasis, repair, and regeneration. ProTracer reveals highly regional proliferation in midzonal hepatocytes, showing its greater contribution to maintaining the hepatocyte pool during liver homeostasis. Additionally, ProTracer revealed highly regional hepatocyte generation during liver repair and regeneration after injuries. Future applications and further iterations of ProTracer could substantially advance our understanding of cell generation and their dynamics in development, growth, regeneration, and diseases in multiple organs. ■

The list of author affiliations is available in the full article online.
*These authors contributed equally to this work.
†Corresponding author. Email: zhoubin@sibs.ac.cn
Cite this article as L. He *et al.*, *Science* **371**, eabc4346 (2021). DOI: 10.1126/science.abc4346

READ THE FULL ARTICLE AT
https://doi.org/10.1126/science.abc4346

RESEARCH ARTICLE

LINEAGE TRACING

Proliferation tracing reveals regional hepatocyte generation in liver homeostasis and repair

Lingjuan He[1]*, Wenjuan Pu[1]*, Xiuxiu Liu[1]*, Zhenqian Zhang[1], Maoying Han[1,2], Yi Li[1], Xiuzhen Huang[1], Ximeng Han[1], Yan Li[1], Kuo Liu[1], Mengyang Shi[1], Liang Lai[3], Ruilin Sun[3], Qing-Dong Wang[4], Yong Ji[5], Jan S. Tchorz[6], Bin Zhou[1,2,7,8]†

Organ homeostasis is orchestrated by time- and spatially restricted cell proliferation. Studies identifying cells with superior proliferative capacities often rely on the lineage tracing of a subset of cell populations, which introduces a potential selective bias. In this work, we developed a genetic system [proliferation tracer (ProTracer)] by incorporating dual recombinases to seamlessly record the proliferation events of entire cell populations over time in multiple organs. In the mouse liver, ProTracer revealed more hepatocyte proliferation in distinct zones during liver homeostasis, injury repair, and regrowth. Clonal analysis showed that most of the hepatocytes labeled by ProTracer had undergone cell division. By genetically recording proliferation events of entire cell populations, ProTracer enables the unbiased detection of specific cellular compartments with enhanced regenerative capacities.

Organ homeostasis is often maintained by highly proliferative cellular compartments that arise from different stem cell populations (*1*–*4*). These specialized progenitor or stem cells have mostly been identified by defined marker genes and through lineage tracing techniques (*5*–*8*). However, using individual markers to define a tissue stem cell might introduce a potential bias, which focuses more on the fates of these marker cells rather than on cell generation at the entire population level. These genetic-fate mapping results lead to conflicting conclusions, as illustrated by the highly controversial studies around cell sources for hepatocyte generation (*9*–*18*). Hepatocytes can be replaced by the conversion of cholangiocytes under severe injury conditions (*19*–*22*); however, the hepatocyte pool is mostly maintained by the proliferation of preexisting hepatocytes during homeostasis and regeneration (*23*). Although hepatocytes in different zones of the liver lobule are heterogeneous in cell proliferation, a key question remains regarding the zonal contribution of different hepatocyte populations to liver homeostasis and regeneration.

It has been proposed that proliferating periportal hepatocytes gradually stream toward the central vein, where they are eventually eliminated (*9*). However, this hepatocyte streaming model with its portal-to-central directionality remains controversial (*10*, *11*), with counter-evidence, such as lineage tracing studies, showing that Axin2$^+$ hepatocytes residing in the pericentral regions of the lobule proliferate in a central-to-portal direction to fuel homeostatic renewal of the liver (*12*). Genetic lineage tracing studies from other groups, however, have suggested that pericentral Axin2$^+$ or Lgr5$^+$ hepatocytes have limited contributions to liver homeostasis and regeneration (*14*, *17*, *18*). Additionally, periportal Sox9$^+$ hepatocytes undergo extensive proliferation and replenish liver mass after liver injury (*13*). Other fate mapping studies have reported that hepatocytes throughout the liver expressing LGR4 contribute to liver homeostasis (*14*) and that hepatocytes in all zones expressing telomerase reverse transcriptase (TERT) have superior proliferate capacity over TERT-negative hepatocytes (*16*), which supports a distributed model of hepatocyte renewal. Clonal analysis of hepatocyte expansion has shown that hepatocytes in all three zones (periportal zone, central zone, and midzonal) contribute to liver homeostasis, with hepatocytes in the midlobular zone proliferating substantially more than hepatocytes in the other zones (*24*). Relying on individual marker genes used for lineage tracing or using sparse labeling might account for the conflicting findings of these studies. Thus, an unbiased assessment of proliferative events in the entire hepatocyte pool over time could shed light on the spatial heterogeneity of hepatocyte generation during liver homeostasis and regeneration.

In this study, we generated a genetic system that permits temporally continuous and tissue-specific recording of cell proliferation in vivo. To highlight its utility, we applied it to study hepatocyte generation during liver homeostasis and regeneration.

Results

Design and generation of genetic recording system for cell proliferation

We first generated a genetic recording system of cell proliferation by fate mapping Ki67-expressing cells over time (Fig. 1A). A widely used marker of cell proliferation is Ki67 (*25*), and two recently reported lineage tracing methods have exploited Ki67 for labeling proliferating cells upon tamoxifen (Tam) treatment (*25*, *26*). Notably, given that the Tam serum half-life in mice is generally 12 to 24 hours (*27*), the Tam-induced Cre activity declines over time, eventually precluding the effective recording of new Ki67$^+$ cells over time (Fig. 1B). Further, it is technically challenging to efficiently maintain constant Cre activity in mice through continuous Tam treatment over several weeks or months, which may have toxicity and adverse effects on tissues (*28*). We therefore envisioned that the approach to trigger a constitutively active Cre-based genetic system in theory should allow us to prime specific cell populations with the ability to continuously record their proliferation.

We developed a genetic strategy to record cell proliferation with only a single initial pulse of Tam treatment that is based on a dual recombinase–mediated genetic system. The genetic design of this system involves three mouse lines: *DreER* (*29*), *Ki67-CrexER* (*Ki67-Cre-rox-ER-rox*), and a *R26-GFP* reporter (*30*) (Fig. 1C). Specifically, Tam-induced DreER-rox recombination is used to excise rox-flanked estrogen receptor (ER) DNA, thereby converting the coding sequence for the inducible CrexER into that for the constitutively active Cre DNA. This ultimately yields a new *Ki67-Cre* genotype in DreER-expressing cells, which primes the system for continuous genetic recording of cell proliferation by Cre-loxP recombination. In such cells, the Ki67 promoter–driven expression of constitutively active Cre permanently records active Ki67 transcription by turning on the aforementioned *R26-GFP* reporter. After turning the system on with one pulse of Tam, it remains on and enables the tracing of Ki67$^+$ cells at any time thereafter—a concept that in theory enables the continuous recording of cell proliferation in any defined time window through an animal's life span. We termed this model ProTracer (proliferation tracer) (Fig. 1C).

We first generated and characterized the *Ki67-CrexER* mouse line. CrexER was inserted

[1]State Key Laboratory of Cell Biology, Shanghai Institute of Biochemistry and Cell Biology, Center for Excellence in Molecular Cell Science, Chinese Academy of Sciences, University of Chinese Academy of Sciences, Shanghai, China. [2]School of Life Science and Technology, ShanghaiTech University, Shanghai, China. [3]Shanghai Model Organisms Center, Inc., Shanghai, China. [4]Bioscience Cardiovascular, Research and Early Development, Cardiovascular, Renal and Metabolism (CVRM), BioPharmaceuticals R&D, AstraZeneca, Gothenburg, Sweden. [5]The Collaborative Innovation Center for Cardiovascular Disease Translational Medicine, Nanjing Medical University, Nanjing, China. [6]Novartis Institutes for BioMedical Research, Novartis Pharma AG, Basel, Switzerland. [7]School of Life Science, Hangzhou Institute for Advanced Study, University of Chinese Academy of Sciences, Hangzhou, China. [8]Institute for Stem Cell and Regeneration, Chinese Academy of Sciences, Beijing, China.
*These authors contributed equally to this work.
†Corresponding author. Email: zhoubin@sibs.ac.cn

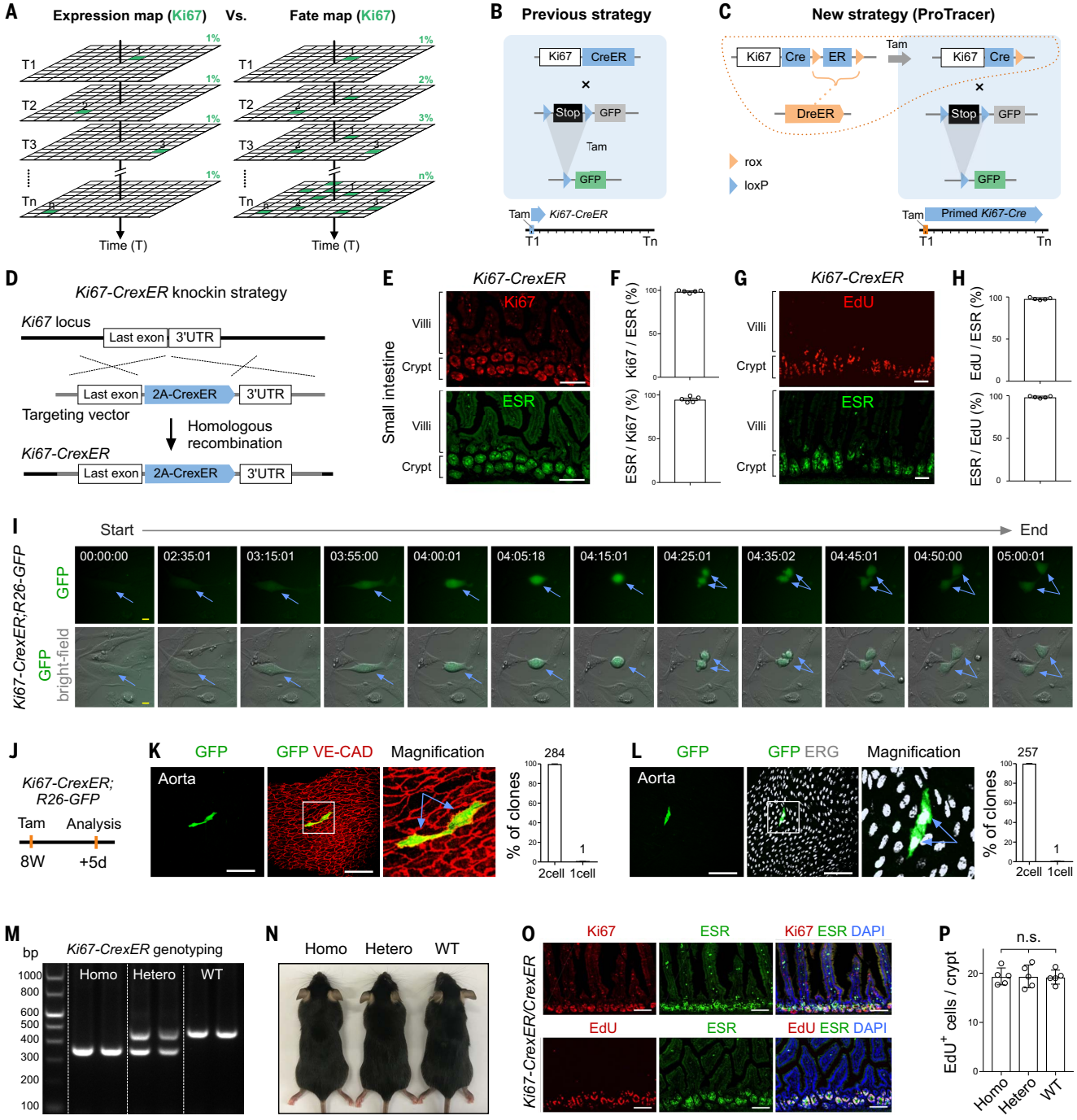

Fig. 1. Generation and characterization of *Ki67-CrexER* mice. (**A**) Schematic showing a Ki67 expression map and fate map. *Ki67* is dynamically expressed from time point 1 (T1) to time point n (Tn), whereas fate mapping of *Ki67* records all cell proliferation events from T1 to Tn. Each green square denotes a Ki67-expressing cell (left) or a Ki67$^+$ cell and progeny (right). (**B**) Schematic showing fate mapping of Ki67$^+$ cells by using *Ki67-CreER;R26-GFP* mice. (**C**) Schematic showing ProTracer strategy. Tam-induced DreER-rox recombination switches CrexER into Cre driven by the *Ki67* promoter, which primes the system to continuously record all cell proliferation events from T1 to Tn. (**D**) Strategy for generation of *Ki67-CrexER* knock-in alleles by homologous recombination with CRISPR-Cas9. (**E** and **G**) Immunostaining for Ki67 (E) or EdU (G) with estrogen receptor (ESR) on small intestine sections from adult *Ki67-CrexER* mice. ESR denotes Ki67 gene expression. (**F** and **H**) Quantification of the percentage of ESR$^+$ cells expressing Ki67 [(F), top] or EdU [(H), top] or the percentage of Ki67$^+$ [(F), bottom] or EdU$^+$ [(H), bottom] cells expressing ESR. Data are means ± SEM; $n = 5$. (**I**) Live imaging of GFP$^+$ cells isolated from *Ki67-CrexER;R26-GFP* embryos; 4-OH Tam was added 6 hours before this analysis. Arrows point to a cell from GFP$^-$ to GFP$^+$ during cell proliferation. (**J**) Examination of the proliferation of aortic endothelial cell using *Ki67-CrexER;R26-GFP* mice. 8W, 8 weeks; 5d, 5 days. (**K** and **L**) Immunostaining for GFP, endothelial cell marker VE-CAD (K), or endothelial nuclei marker ERG (L) in the aortic endothelium. Blue arrows indicate pairs of endothelial cells. A quantification of the percentages of two-cell or one-cell GFP$^+$ signals is shown (right). (**M**) Polymerase chain reaction (PCR) of genomic DNA shows homo (*Ki67-CrexER/CrexER*), hetero (*Ki67-CrexER/+*), and wild-type (WT) (*Ki67 +/+*) mice. (**N**) Images showing 10-week-old mice of three genotypes. (**O**) Immunostaining for Ki67, EdU, and ESR on intestine sections of adult homo (*Ki67-CrexER/CrexER*) mice. DAPI, 4′,6-diamidino-2-phenylindole. (**P**) Quantification of EdU$^+$ cells per crypt of small intestine. Data are means ± SEM; $n = 5$. n.s., nonsignificant. Scale bars: white, 100 μm; yellow, 10 μm. Each image is representative of five individual biological samples.

into the 3′ untranslated region (3′UTR) of the *Ki67* gene using the self-cleaved peptide P2A (Fig. 1D). Confirming that CrexER expression accurately mirrored Ki67 expression, the co-staining of Ki67 and ESR (a surrogate for CrexER) revealed highly similar expression patterns in the intestinal epithelium of adult *Ki67-CrexER* mice (Fig. 1, E and F). Independently, we injected EdU into *Ki67-CrexER* mice 3 hours before tissue collection to detect DNA synthesis during cell proliferation and found similar patterns with CrexER expression and EdU labeling (Fig. 1, G and H). To examine the specificity and fidelity of *Ki67-CrexER* for tracing cell proliferation, we used both in vitro live imaging experiments and in vivo clonal analysis of labeled cells. To confirm the utility of this *Ki67-CrexER* allele as a representative marker of cell proliferation, we isolated cells from *Ki67-CrexER;R26-GFP* tissues and monitored their proliferation in in vitro cell cultures (Fig. 1I). CrexER works in the same way as CreER for Cre-loxP recombination after Tam (*31*), except that CrexER can be switched into Cre upon Dre-rox recombination (*31*). Live imaging revealed green fluorescent protein (GFP) expression in proliferating cells by in vitro cell culture with Tam: Single cells expressed GFP and underwent cell division (Fig. 1I). We observed that 131 of 133 GFP^+ cells had undergone cell proliferation (one cell divided into two), which indicates the specificity of Ki67-based lineage tracing for recording cell proliferation. To address the specificity of ProTracer for in vivo cell proliferation, we examined the aorta endothelial cells of *Ki67-CrexER;R26-GFP* mice: Three dimensional (3D) whole-mount imaging of the aorta revealed that GFP^+ endothelial cells almost invariably occurred as pairs, and the endothelial cells in each pair were closely contacting each other (Fig. 1, J to L). Additionally, our *Ki67-CrexER* allele maintains endogenous Ki67 expression and functions, as homozygous *Ki67-CrexER* mice showed growth, tissue morphologies, and cell proliferation similar to those of their littermate heterozygous or wild-type controls (Fig. 1, M to P; fig S1; and fig. S2, A and B). EdU incorporation was also detected in GFP^+ hepatocytes labeled by ProTracer (fig. S2, C and D). Collectively, these results establish that our *Ki67-CrexER* allele can faithfully and specifically record Ki67-associated cell proliferation.

ProTracer efficiently records in vivo cell proliferation

By crossing *R26-DreER* (*29*) and *Ki67-CrexER; R26-GFP* mice, we generated ProTracer mice for the genetic recoding of cell proliferation in most organs and tissues (Fig. 2A). One pulse of Tam-induced DreER-rox recombination should excise ER and thus switch *Ki67-CrexER* into *Ki67-Cre* (Fig. 2A), priming the ProTracer system for recording cell proliferation. Southern blotting of genomic DNA from multiple tissues revealed *Ki67-CrexER*–to–*Ki67-Cre* genotype switching at rates ranging from ~50 to ~100% in diverse tissues, with the highest rate observed in the liver (Fig. 2B). We then examined ProTracer mice using whole-mount fluorescence and immunostaining of GFP activity at 2 and 28 days after the initial Tam activation of the recording system (Fig. 2C). Therefore, the GFP signal we observed in the ProTracer organs only results from Cre-loxP recombination in $Ki67^+$ cells. To facilitate comparison of our ProTracer system with a previously reported cell proliferation tracing technique, we also generated *Ki67-CreER;R26-GFP* mice (Fig. 2C). At day 2 after Tam activation, all examined tissues (except the highly proliferative intestinal epithelium) in both the ProTracer and the *Ki67-CreER;R26-GFP* mice exhibited rare GFP signals (Fig. 2D). Contrastingly, by day 28 after Tam activation, whole-mount and sectional analyses revealed more-intense GFP signals in the ProTracer mice compared with the *Ki67-CreER;R26-GFP* mice—a result that emphasizes the capacity of ProTracer to continuously activate GFP reporter expression upon new cell-division events (Fig. 2E).

As technical controls, we detected very few GFP^+ cells in *Ki67-CreER;R26-GFP* mice, ProTracer mice without Tam treatment (fig. S3 and fig. S4), or the *R26-DreER;R26-GFP* mice treated with Tam (fig. S5). Therefore, the detection of GFP^+ cells in different organs or tissues from Tam-treated ProTracer mice (Fig. 2, D and E) relies on both DreER-rox recombination and subsequent Cre-loxP recombination. Collectively, these results highlight the temporally continuous nature of ProTracer, which permits the recording of ongoing cell proliferation events in diverse organs.

ProTracer-based identification of regional hepatocyte proliferation during homeostasis

Given its capacity to record cell proliferative events, and considering the heterogeneity of hepatocytes during liver homeostasis (*32*), we applied ProTracer to simultaneously monitor all of the hepatocyte populations and to examine the possible sources (e.g., subpopulations of hepatocytes) and locations for new hepatocyte generation. The liver lobule is divided into three distinct zones (*32*, *33*), and molecular markers have been used to demarcate them (*34*). These three distinct zones are the periportal zone surrounding the portal vein [marked by E-cadherin (E-CAD)], which is defined as zone 1 in this study; the central zone nearest to the central vein, or zone 3 [marked by glutamine synthetase (GS)]; and zone 2, which consists of the midzonal hepatocytes in between zones 1 and 3 (*35*) (Fig. 3A). We used Tam to induce the DreER-rox–mediated switch of *Ki67-CrexER* into the *Ki67-Cre* genotype, priming ProTracer for cell proliferation recording (Fig. 3B). Southern blotting of isolated hepatocytes showed that *Ki67-CrexER* was switched to *Ki67-Cre* in virtually all hepatocytes in Tam-treated but not corn oil–treated ProTracer mice (Fig. 3B). We also examined whether *R26-DreER* recombined hepatocytes uniformly throughout the liver lobule by crossing it with R26-rox-Stop-rox-tdTomato rox reporter mice (*R26-RSR-tdTomato*) (*36*) and found that *R26-DreER* recombined almost all hepatocytes in the liver after Tam (fig. S6).

We euthanized mice, collected liver samples at different time points, and examined in situ hepatocyte proliferation in the homeostatic liver lobule (Fig. 3C). Immunostaining for GFP, GS, E-CAD, and β-catenin (cell membrane marker) showed either no or rare GFP^+ hepatocytes on liver sections at days 0 and 2, respectively (Fig. 3D); more GFP^+ hepatocytes were observed from weeks 2 to 8, with pronounced enrichment in zone 2 (Fig. 3E). We did detect increased numbers of GFP^+ hepatocytes in zone 1 in the period between weeks 8 and 12, but the numbers of hepatocytes were still significantly lower than those of zone 2 (Fig. 3, E and F). The significantly higher number of GFP^+ hepatocytes in the midzone of the liver lobule indicates more hepatocyte generation in this region. Quantification of the percentage of GFP^+ hepatocyte–increase per week at five time windows (weeks 2 to 4, 4 to 6, 6 to 8, 8 to 10, and 10 to 12) revealed the proliferation rate of the hepatocytes in each zone (Fig. 3F, inset), which suggests an approximate hepatocyte proliferation rate of 0.042 per week in zone 2 during homeostasis (Fig. 3F). It was notable that the percentage of GFP^+ hepatocytes was significantly lower in zone 3 between weeks 2 and 12, compared with zones 1 and 2 (Fig. 3, E and F). We then used a *GS-CreER* driver to independently examine whether hepatocytes in zone 3 expand significantly during liver homeostasis. By using *GS-flagBFP* and *GS-CreER* knock-in lines (fig. S7), we confirmed that GS was specifically expressed in pericentral hepatocytes (zone 3). For an unknown reason, this *GS-CreER* specifically labeled GS^+ hepatocytes without Tam. However, genetic lineage tracing of these GS^+ hepatocytes (zone 3) revealed that they had not expanded significantly by 8 weeks (fig. S7). Both lineage tracing and ProTracer data indicate that pericentral (zone 3) hepatocytes do not expand significantly during liver homeostasis. Taken together, continuous proliferation recording of all hepatocyte populations suggests that hepatocyte proliferation rates are highest in zone 2, modest in zone 1, and lowest in zone 3 during liver homeostasis.

Hepatocyte-specific ProTracer reveals distinct donut-shaped proliferation pattern

Although hepatocytes in the adult liver have been assumed to be derived from preexisting hepatocytes through proliferation (*37*–*39*), recent

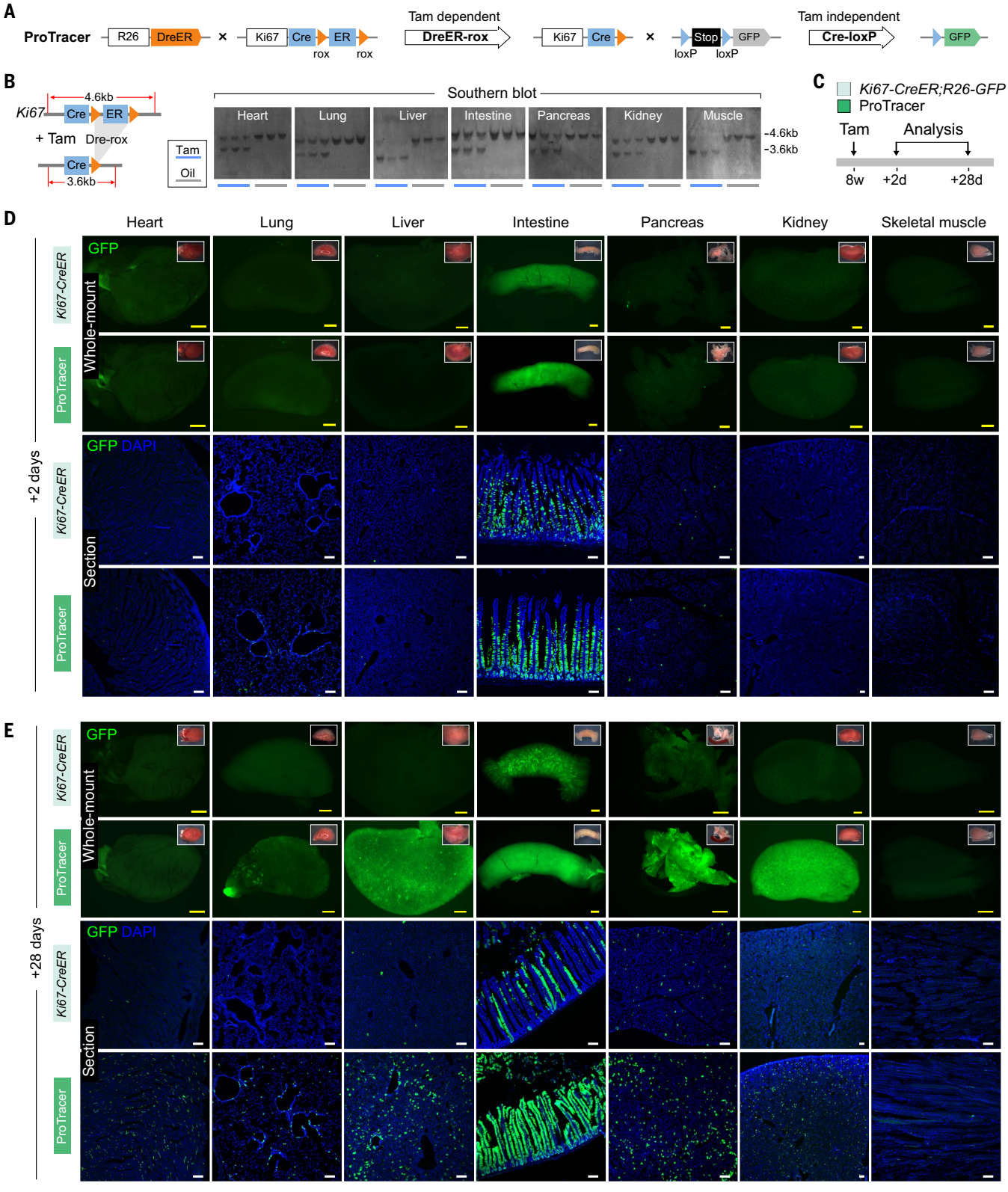

Fig. 2. Tracing cell proliferation in multiple organs and tissues by ProTracer. (**A**) Schematic showing ProTracer primed by DreER-rox recombination. The ProTracer mouse used here is *R26-DreER;Ki67-CrexER;R26-GFP*. (**B**) Schematic figure showing Southern blotting analysis of various tissues from ProTracer mice. Tam, tamoxifen induction; Oil, corn oil–treated ProTracer mice as control group. (**C**) Schematic showing the experimental strategy used to compare the efficiency of the *Ki67-CreER;R26-GFP* and ProTracer strategies for the tracing of cell proliferation. (**D** and **E**) Whole-mount GFP fluorescent images of organs and immunostaining for GFP on tissue sections prepared from the indicated organs of *Ki67-CreER;R26-GFP* (*Ki67-CreER*) or ProTracer mice at 2 days (D) or 28 days (E) after Tam treatment. Scale bars: yellow, 1 mm; white, 100 μm. Each figure is representative of five individual biological samples.

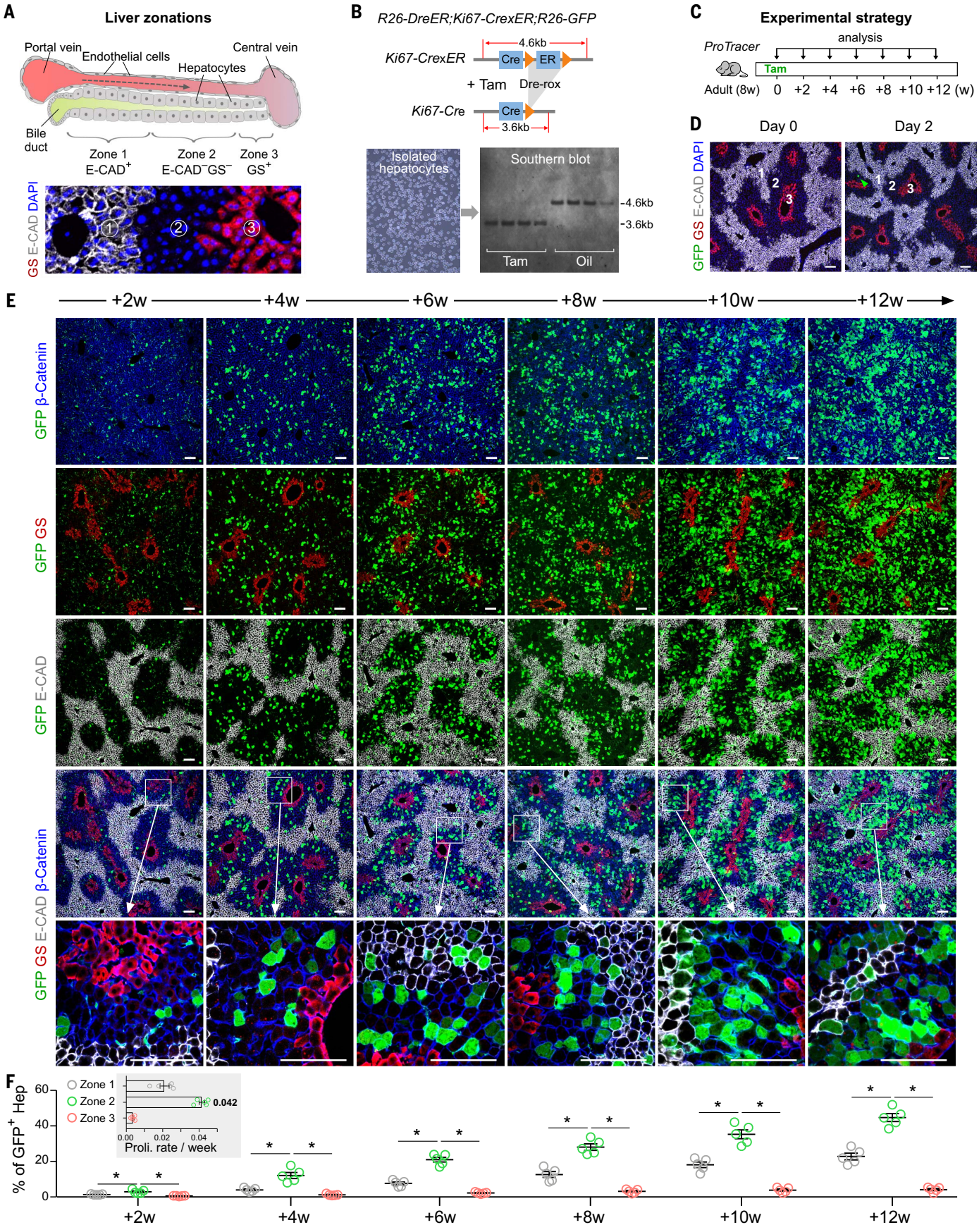

Fig. 3. ProTracer reveals highly regional hepatocyte proliferation in the liver lobule. (**A**) Schematic showing three liver zones from the periportal to the pericentral region. Lower panel shows immunostaining for glutamine synthetase (GS) and E-cadherin (E-CAD). 1, 2, and 3 indicate zone 1 (E-CAD$^+$), zone 2 (E-CAD$^-$GS$^-$), and zone 3 (GS$^+$), respectively. Dashed arrow indicates blood flow. (**B**) Schematic showing the strategy used to detect floxed ER DNA excision in isolated hepatocytes using Southern blotting. The lower panel shows Southern blots of hepatocyte DNA collected from Tam- or oil-treated ProTracer mice. (**C**) Schematic showing the experimental strategy using ProTracer (*R26-DreER;Ki67-CrexER;R26-GFP*). (**D**) Immunostaining for GFP, GS, and E-CAD on liver sections at baseline (day 0) and day 2 after Tam treatment. Arrowhead indicates GFP$^+$ hepatocyte. (**E**) Immunostaining for GFP, GS, E-AD, and β-catenin on liver sections collected at weeks 2, 4, 6, 8, 10, and 12 after Tam treatment. (**F**) Quantification of the percentage hepatocytes (Hep) expressing GFP in each zone of the liver lobule. Data are means ± SEM; $n = 5$. *$P < 0.05$. Inset is proliferation (proli.) rate of hepatocytes per week from five time windows (weeks 2 to 4, 4 to 6, 6 to 8, 8 to 10, and 10 to 12) in each zone. Scale bars, 100 μm. Each figure is representative of five individual biological samples.

studies have suggested that biliary epithelial cells or ductal cells may also contribute to new hepatocytes under some special conditions (*19*–*22*, *40*). Additionally, *R26-DreER*–primed ProTracer targets all types of cells (e.g., endothelial cells, fibroblasts, macrophages, etc.), which obscures the detection of distinct patterning for hepatocyte proliferation in the liver lobules. To more clearly discern the regional cell proliferation patterning from whole organs, and to specifically monitor the hepatocyte populations, we next modified the ProTracer system to enable cell lineage–specific proliferation tracing. We used another dual recombinase–mediated genetic strategy to achieve tissue-specific ProTracer recording. As a proof of concept, and aiming to specifically record proliferating hepatocytes, we crossed *Alb-DreER* (*41*) with *Ki67-CrexER* mice and with dual recombinase–activated reporter *Ai66* mice (*42*) (Fig. 4A). *Alb-DreER* recombined hepatocytes in all three zones efficiently after Tam injection (fig. S8A). We anticipated that Tam-induced DreER-rox recombination would excise both rox-ER-rox from the *Ki67-CrexER* and rox-stop-rox from the *Ai66*, genetically generating *Ki67-Cre* and *R26-LSL-tdTomato* genotypes specifically in albumin (Alb)–expressing hepatocytes (Fig. 4A). Subsequently, upon any hepatocyte proliferation event, *Ki67-Cre* should excise loxP-stop-loxP from the *R26-LSL-tdTomato*, leading to constitutive tdTomato expression only in Alb$^+$Ki67$^+$ hepatocytes (Fig. 4A). Immunostaining for tdTomato and cell lineage markers on liver sections of *Alb-DreER;Ki67-CrexER;Ai66* mice revealed that all tdTomato$^+$ cells were verified as FAH$^+$ and HNF4α$^+$ hepatocytes; no tdTomato signal was detected in CK19$^+$ ductal cells, Desmin$^+$ stellate cells, PDGFRa$^+$ fibroblasts, VE-CAD$^+$ endothelial cells, or F4/80$^+$ macrophages (>1000 cells of each cell type were counted in each sample; Fig. 4, B and C). This confirms that proliferation of only hepatocytes, but not of any other cell lineages, was genetically recorded by hepatocyte-specific ProTracer.

We next collected livers from *Alb-DreER;Ki67-CrexER;Ai66* mice at 6 weeks after Tam-induced activation of the ProTracer system. Whole-mount fluorescence imaging of the livers showed that the hepatocyte-specific tdTomato$^+$ signal occurred as a donut-shaped pattern (Fig. 4D). This increase of resolution for visualizing proliferation patterning from whole-mount organs was likely a result of hepatocyte-only signals, as hepatocyte-specific ProTracer did not record the proliferation of other cell lineages (Fig. 4, A to C). 3D whole-mount fluorescence imaging of livers by light-sheet microscopy revealed distinct circular patterning for tdTomato$^+$ signals (Fig. 4E and movie S1), reinforcing the highly regional hepatocyte generation in homeostatic liver lobules. Immunostaining of liver sections with antibodies against tdTomato, GS, E-CAD, and β-catenin supported this highly regional pattern and indicated that the majority of hepatocyte proliferation activity occurred in zone 2 (Fig. 4F). Quantification data showed a significantly higher percentage of tdTomato$^+$ hepatocytes in zone 2 than in zones 1 or 3 (Fig. 4G). As a technical control, we observed very rare tdTomato$^+$ hepatocytes in livers collected from *Alb-DreER;Ki67-CrexER;Ai66* mice without Tam (fig. S8, B and C). These data demonstrated that zone 2 was the region with the highest homeostatic hepatocyte proliferation, which might be responsible for the donut-like pattern observed in whole-mount liver images.

To avoid potential bias introduced by Tam injections, we next activated the ProTracer system (*Ki67-CrexER;R26-GFP*) with AAV8-TBG-Dre (AAV8-Dre), which is known to have a strong hepatocyte tropism (*37*) (Fig. 4H). By both *R26-RSR-GFP* and *R26-RSR-tdTomato* reporters, AAV8-Dre efficiently targeted hepatocytes in all zones (fig. S9). Eight weeks after AAV8-Dre injection, all GFP$^+$ cells were positive for hepatocyte-specific markers HNF4α and FAH, which demonstrates hepatocyte-specific labeling in AAV8-Dre–induced *Ki67-CrexER;R26-GFP* mice (Fig. 4I). Immunostaining for GFP, E-CAD, GS, and β-catenin on liver sections revealed that the majority of GFP$^+$ hepatocytes were located in zone 2, whereas significantly fewer GFP$^+$ hepatocytes were found in zones 1 or 3 (Fig. 4J), which reinforces the observation of the regional midzonal hepatocyte generation during liver homeostasis.

We also explored whether ProTracer could be extended for noninvasive monitoring of gradual hepatocyte proliferation recording events in live mice over the course of long-term studies (e.g., weeks to months). We replaced the fluorescence reporter mice with *R26-Luciferase* mice and achieved hepatocyte-specific ProTracer activation with AAV8-Dre (*37*) (Fig. 4K). After AAV8-Dre–induced ProTracer activation, biweekly monitoring of luciferase signals in the same live mouse showed a gradual increase of luciferase activity in the AAV8-Dre– but not the AAV8-control–injected mice (Fig. 4L), demonstrating a gradual increase of hepatocyte-specific proliferation recording events over time. These data further suggest that the donut-like pattern (Fig. 4, D to F) was a result of the accumulation of gradual hepatocyte proliferation events during long-term recording in tissue homeostasis.

Most Ki67$^+$ hepatocytes labeled by ProTracer have undergone cell division

Hepatocytes are polyploid and binuclear (*43*), and they do not always undergo cell division (*44*, *45*). Therefore, cell-cycling marker expression such as Ki67 may not necessarily indicate complete cell division but might also mark polyploidization events without complete cell cycle progression. To determine the percentage of Ki67$^+$ cells labeled by ProTracer undergoing cell division versus polyploidization, we injected *Ki67-CrexER;R26-GFP* mice with low-dose AAV8-Dre for sparse GFP labeling of Ki67$^+$ hepatocytes (Fig. 5, A and B). In this sparse labeling, pairs of neighboring GFP$^+$ hepatocytes indicate homeostatic cell division, whereas individual GFP$^+$ hepatocytes with two or more nuclei indicate polyploidization without cell division. To faithfully detect these events in the 3D liver lobule, we analyzed multiple Z stacks on 50- to 100-μm liver sections (Fig. 5C). Z-stacked confocal images of liver sections immunostained for GFP and β-catenin revealed that the majority of GFP$^+$ clusters exhibited a pair of neighboring hepatocytes (Fig. 5, D and E). Serial section analysis (Fig. 5F) and quantification data (Fig. 5G) showed that ~90% of GFP$^+$ hepatocytes were in clusters of two or more cells, with minimal contribution of individual (singlet) hepatocytes. Again, most of these pairs of hepatocytes were observed in zone 2 of the liver lobule (Fig. 5H). We confirmed this result by more sparse labeling experiments with further-reduced AAV8-Dre doses (Fig. 5I). Additionally, we crossed *Alb-DreER;Ki67-CrexER* with *Ai66* reporter and collected mice at 4 weeks after low dosage of Tam treatment. Clonal analysis showed that the majority of tdTomato$^+$ clones have two

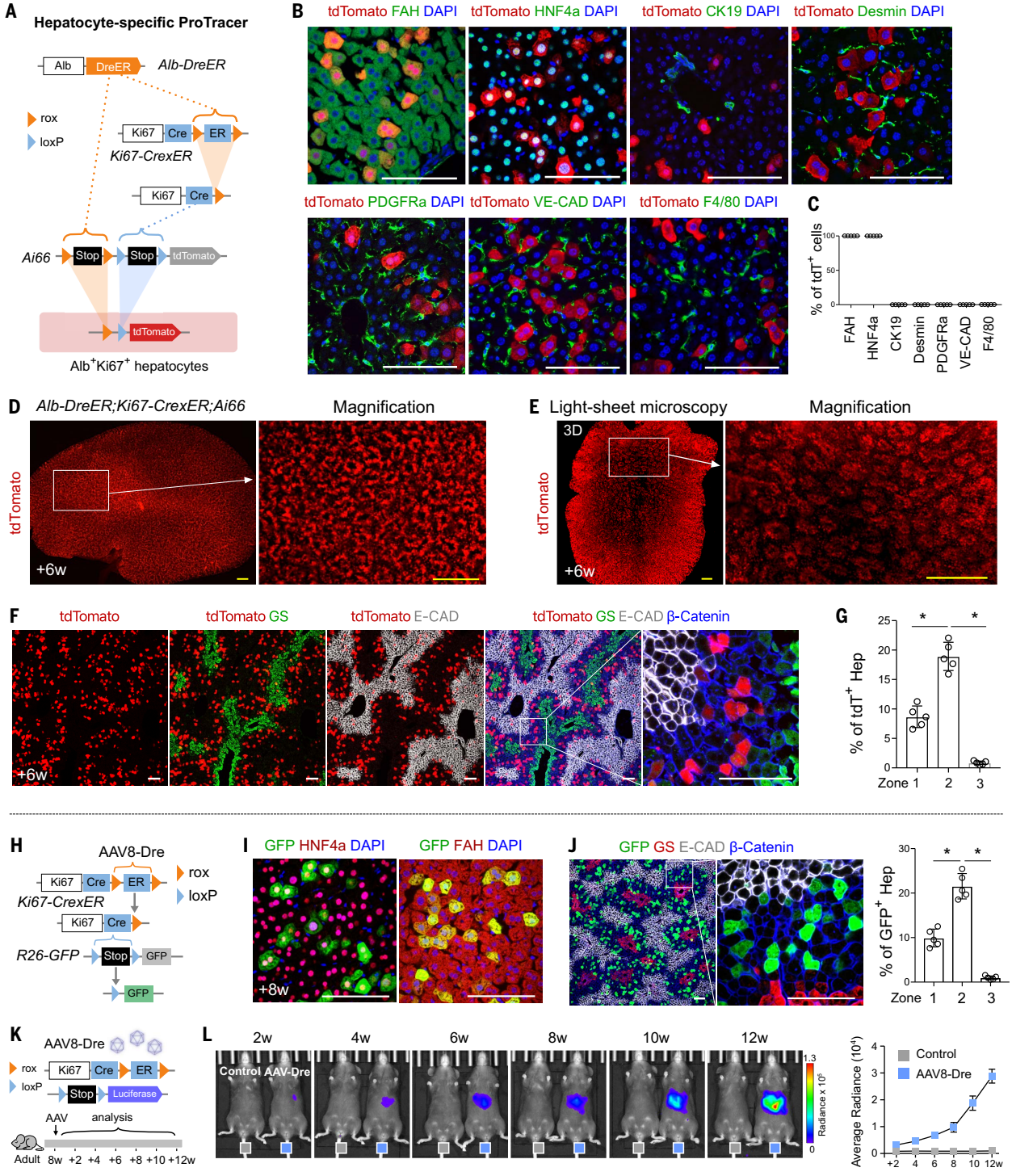

Fig. 4. Hepatocyte-specific ProTracer identifies highly regional hepatocyte generation during homeostasis. (**A**) Schematic showing the experimental strategy used for hepatocyte-specific tracing of cell proliferation. (**B**) Immunostaining for tdTomato, FAH, HNF4a, CK19, Desmin, PDGFRa, VE-CAD, and F4/80 on liver sections. Tissues were collected at 6 weeks after Tam induction. (**C**) Quantification of the percentage of tdTomato$^+$ (tdT$^+$) cells expressing different cell lineage markers. (**D**) Whole-mount fluorescence image of liver collected from hepatocyte-specific ProTracer mouse at 6 weeks after Tam induction. (**E**) 3D light-sheet microscopic image showing donut-like tdTomato signals in liver. (**F**) Immunostaining for tdTomato, GS, E-CAD, and β-catenin on liver sections. (**G**) Quantification of the percentage of hepatocytes expressing tdTomato in each zone of the liver lobule. Data are means ± SEM; $n = 5$. *$P < 0.05$. (**H**) Schematic showing AAV8-Dre–induced hepatocyte-specific ProTracer system. (**I**) Immunostaining for GFP, HNF4a, or FAH on liver sections. (**J**) Immunostaining for GFP, E-CAD, GS, and β-catenin on liver sections. A quantification of the percentage hepatocytes (Hep) expressing GFP in each zone of the liver lobule (right) is shown. Data are means ± SEM; $n = 5$. *$P < 0.05$. (**K**) Schematic showing an AAV8-Dre–induced hepatocyte-specific ProTracer system using luciferase reporter as readout. (**L**) Bioluminescence imaging of the same mice from 2 to 12 weeks after AAV induction and quantification data showing luciferase activity. Data are means ± SEM; $n = 5$. AAV8 virus without Dre cDNA was used as a control. Scale bars: yellow, 1 mm; white, 100 μm. Each figure is representative of five individual biological samples.

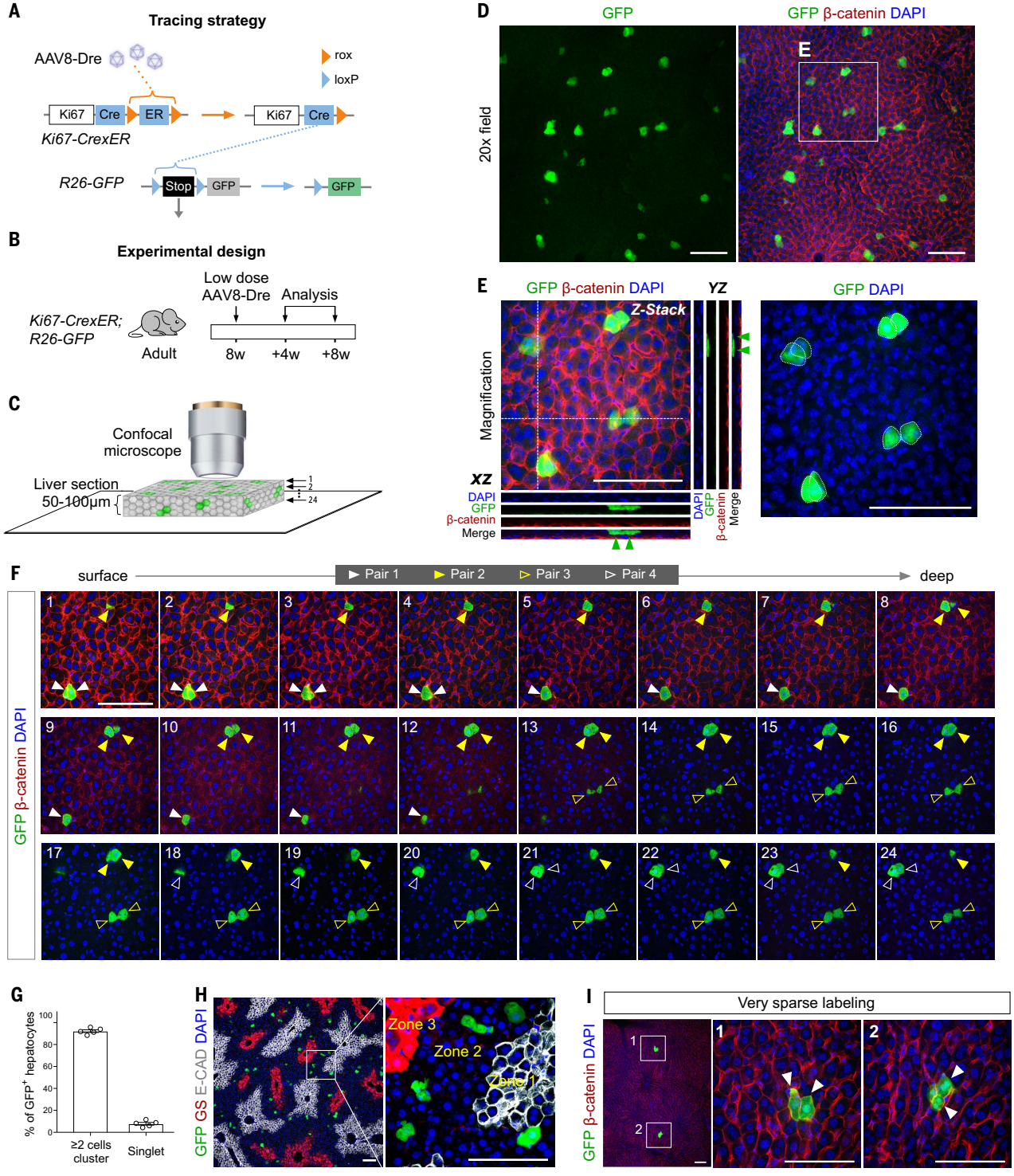

Fig. 5. Most Ki67$^+$ hepatocytes labeled by ProTracer have undergone cell division. (**A**) Schematic showing strategy of labeling Ki67$^+$ hepatocytes by AAV8-Dre injection into *Ki67-CrexER;R26-GFP* mice. (**B**) Schematic showing experimental design for clonal analysis with low dose AAV8-Dre. (**C**) Confocal microscopy of thick liver sections (50 to 100 μm). Each stacked image is composed of 24 layers of scanned signals. (**D**) Immunostaining for GFP and β-catenin on liver sections. Boxed region is magnified in (E). (**E**) Z stack confocal image showing pairs of GFP$^+$ hepatocytes. *XZ* and *YZ* indicate signals from dotted lines on Z stack images. Green arrowheads indicate pairs of GFP$^+$ hepatocytes. Dotted circles in the right panel indicate the border of individual hepatocytes in each clone. (**F**) Serial section analysis (1 to 24 layers, from the surface to a deep layer of section) shows four clusters in this field. Each cluster has a pair of hepatocytes (arrowheads). (**G**) Quantification on the percentage of GFP$^+$ hepatocytes contributed from a cluster of two or more cells or a cluster of single cells (singlets) from five mice samples. Statistical significance is analyzed by binomial test; $P < 0.001$. (**H**) Immunostaining for GFP, GS, and E-CAD on tissue sections. (**I**) Immunostaining for GFP and β-catenin on liver sections collected from *Ki67-CrexER;R26-GFP* mice treated with very low dose AAV8-Dre. Arrowheads indicate hepatocytes. Scale bars, 100 μm. Each image is representative of five individual biological samples.

hepatocytes (fig. S10), which confirms that Tam-induced ProTracer primarily labels proliferating hepatocytes. The above data demonstrated that the majority of Ki67$^+$ hepatocytes labeled by ProTracer have undergone cell division.

Ccna2-based ProTracer revealed highly regional hepatocyte proliferation

To corroborate the above observation, we generated an alternative ProTracer system using a second cell-cycle gene *Ccna2*, which has previously been used for genetically monitoring cell proliferation (*46*). We generated a *Ccna2-CrexER* mouse allele by inserting a CrexER cassette into the endogenous *Ccna2* gene before the 3′UTR by homologous recombination using CRISPR-Cas9, thereby maintaining the endogenous Ccna2 expression. Similar to our Ki67-based ProTracer strategy, Tam-induced Dre-rox recombination switched *Ccna2-CrexER* into the *Ccna2-Cre* genotype, priming the Ccna2-based ProTracer system for genetic recording of cell proliferation (fig. S11A). We injected Tam into *R26-DreER;Ccna2-CrexER;R26-GFP* mice and collected livers for analysis 6 weeks later (fig. S11B). Immunostaining for antibodies against GFP, E-CAD, GS, and β-catenin on the liver sections showed that GFP was more noticeable in zone 2 (fig. S11C). Quantification showed a significantly higher rate of hepatocyte proliferation in zone 2 compared with zones 1 and 3 (fig. S11D).

To further enable Tam-independent and hepatocyte-specific Ccna2-based ProTracer analysis, we injected *Ccna2-CrexER;R26-GFP* mice with AAV8-Dre virus (fig. S11E) and collected livers 12 weeks later (fig. S11F). Whole-mount fluorescence images of *Ccna2-CrexER;R26-GFP* livers showed enriched circular patterns for GFP$^+$ signals (fig. S11G). Immunostaining for GFP, E-CAD, GS, and β-catenin on liver sections showed more GFP$^+$ hepatocyte signals in zone 2 when compared with those in zones 1 or 3 (fig. S11H). Quantification data revealed that the density of GFP$^+$ hepatocytes was highest in zone 2 and lowest in zone 3 (fig. S11I), consistent with our Ki67-based ProTracer data. Collectively, ProTracer-based genetic tracing of cell proliferation (both Ki67 and Ccna2) indicates spatial heterogeneity of hepatocyte proliferation during liver homeostasis and uncovers a highly regional hepatocyte proliferation in the midzonal liver lobule.

Hepatocyte proliferation examined by ProTracer during liver regeneration

Hepatocytes in the adult liver have a notable regenerative capacity upon injury, replacing damaged hepatocytes and maintaining liver mass through induced proliferation (*3*). To systematically investigate regional differences in new hepatocyte generation during liver regeneration, we recorded hepatocyte proliferation events in ProTracer mice during the repair process from different liver injuries. We first performed a partial hepatectomy (PHx) model—an injury model not introducing zonal bias by locally confined damage (*47*)—to examine hepatocyte proliferation during liver regrowth. We induced PHx immediately after Tam induction in ProTracer mice (based on *R26-DreER*) and analyzed livers at 24 hours, 40 hours, 48 hours, 3 days, 4 days, and 7 days after PHx (Fig. 6A). Whole-mount fluorescence images showed increased GFP$^+$ signals in the livers collected from 1 to 7 days after PHx (Fig. 6B). We next performed immunostaining for GFP, GS, E-CAD, and β-catenin on the liver sections (Fig. 6C). At 24 hours, there were very few GFP$^+$ hepatocytes in the liver sections (Fig. 6C). At 40 hours, we noticed a profound increase of GFP$^+$ hepatocytes in zone 1 that was significantly higher than the increases observed in zones 2 and 3 (Fig. 6, C and D), which was detected consistently in different locations of the remaining liver lobes after PHx (fig. S12). At 48 hours, there was a notable increase of GFP$^+$ hepatocytes in both zones 1 and 2, with a minimal increase in zone 3 (Fig. 6, C and D). At 3 and 4 days, more GFP$^+$ hepatocytes were observed in zone 2 than in zone 1 (Fig. 6, C and D). At 3, 4, and 7 days, we detected a noticeable progressing increase of GFP$^+$ hepatocytes in zone 3 (Fig. 6, C and D). These data suggested that hepatocyte regeneration initiated in zone 1 and progressed through zone 2 toward zone 3 after PHx. Additionally, we used hepatocyte-specific ProTracer and obtained similar observation for hepatocyte proliferation that initiates in zone 1 and progresses through zones 2 and 3 after PHx (fig. S13). The cumulative recording with ProTracer further reveals that zone 2 hepatocytes proliferate more during the peak regenerative response within the first 72 hours, whereas, overall, hepatocytes in zones 2 and 1 contributed equally to liver regrowth (both >80% at day 7). By contrast, pericentral hepatocytes in zone 3 show significantly less proliferation within 7 days after PHx. ProTracer provides a high-resolution illustration of hepatocyte proliferation in different zones after PHx, which suggests that liver regeneration occurs in the form of a regenerative wave that initiates in zone 1 and progresses through zone 2 toward zone 3, extending findings from previous studies (*18*, *48*–*52*). Additionally, examination of GFP$^+$ cells in cholangiocytes, endothelial cells, hepatic stellate cells, and macrophages suggested different proliferation dynamics of these nonparenchymal liver cells after PHx (fig. S14). Although macrophages seem to start proliferating earlier than hepatocytes, endothelial cells and cholangiocytes proliferate after the peak proliferation phase of hepatocytes (fig. S14). Together, these data extend previous findings on the proliferative wave of liver cells during liver regrowth and their multicellular dynamics that enable liver regeneration.

To record proliferation events during regeneration after zonal liver injury in zone 3, we subjected ProTracer (based on *R26-DreER*) mice to carbon tetrachloride (CCl_4), which causes acute injury of zone 3 hepatocytes. At days 2, 4, and 7 after CCl_4 treatment, we collected liver samples from ProTracer mice for analysis (fig. S15A). Whole-mount fluorescence images showed increased GFP$^+$ signals in the livers from days 2 to 7 after CCl_4 treatment (fig. S15B). Immunostaining for GFP, GS, E-CAD, and β-catenin on liver sections showed enriched GFP$^+$ hepatocytes in zone 2 at days 2 and 4 after CCl_4 treatment (fig. S15, C and D). At day 7, the majority of hepatocytes in zones 2 and 3 were GFP$^+$ (fig. S15E). Considering the fact that CCl_4 mainly results in hepatocyte death in zone 3, it is likely that zone 2 hepatocytes pioneer the repair process at day 2 and compensate for the loss of zone 3 hepatocytes from days 4 to 7. Additionally, we subjected ProTracer mice to bile duct ligation (BDL) as a zone 1 injury model and collected livers for analysis at days 3, 4, and 7 after BDL (fig. S16, A and B). We found GFP$^+$ hepatocytes were also highly enriched in zone 2 in the BDL model, which exhibited injury in the periportal region with induced ductal reaction (fig. S16, C and D). Together, these data also suggest that there is highly regional hepatocyte generation during liver repair and regeneration after injuries. Recapitulating regenerative processes by continuous proliferation recording highlights the value of our ProTracer system for studying regeneration in multiple organs and injury models.

Discussion

This work illustrates a genetic approach for monitoring and recording in vivo cell proliferation events during tissue homeostasis and regeneration. There are four distinct features of the ProTracer strategy that merit emphasis. First, it allows continuous temporal recording of ongoing cell proliferation (Fig. 1C), thereby enabling long-term studies (months to years; actually throughout the lifetime of a given cell after initial activation of its ProTracer system). Prolonged treatment of DNA analogs such as BrdU or EdU have been shown to induce toxicity and impair proliferation (*53*, *54*). By contrast, ProTracer does not require continued treatment of drugs such as Tam, as an initial Tam pulse primes the genetic system for recording cell proliferation over time. Second, it could be used for studying the proliferation of one specific cell lineage. This capacity should be particularly beneficial for studying cell types that only extremely rarely undergo proliferation (e.g., cardiomyocytes or neurons). In contrast to chemical and immunostaining-based

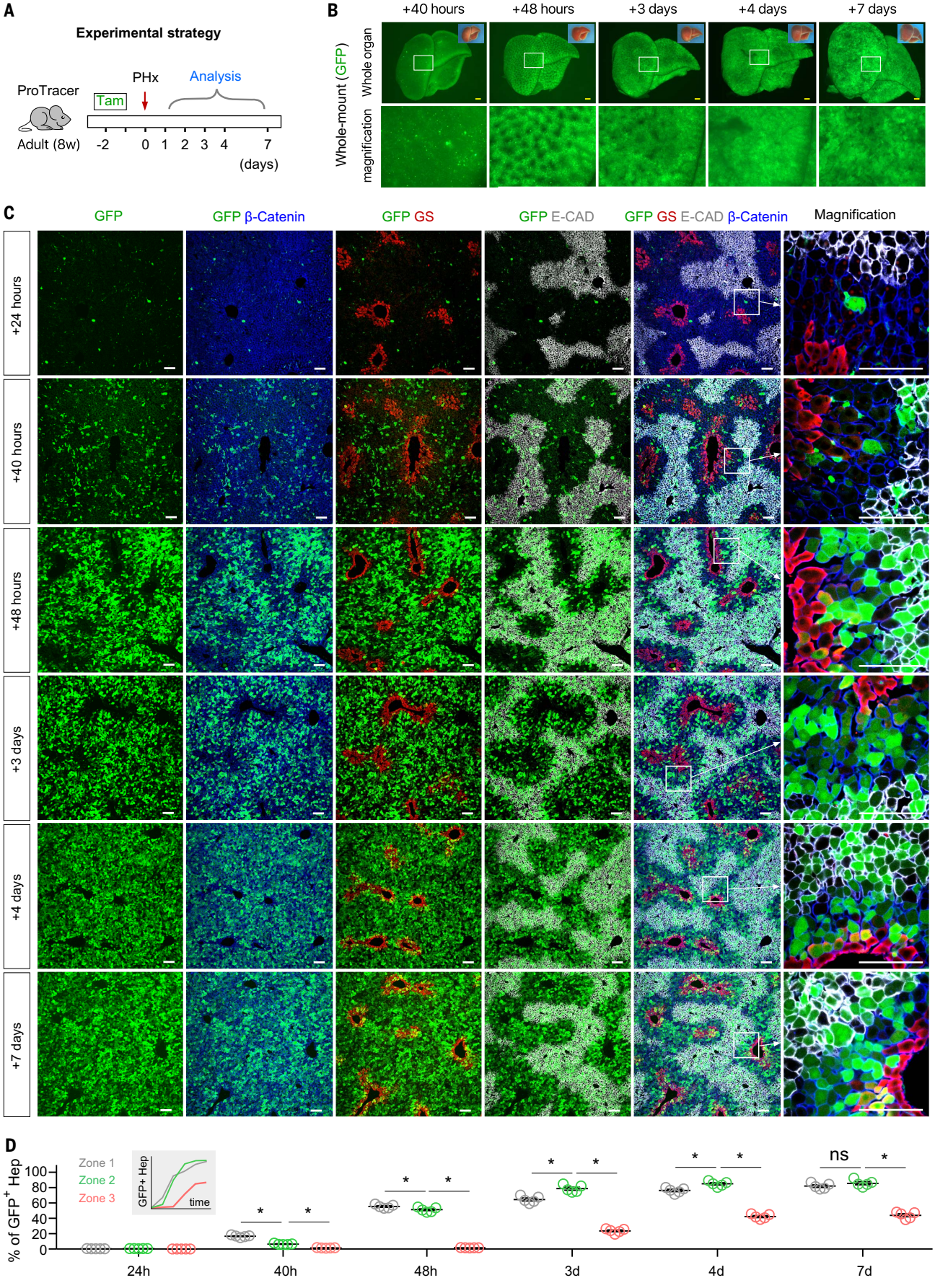

Fig. 6. Genetic tracing of hepatocyte proliferation by ProTracer after PHx. (**A**) Schematic figure showing experimental strategy for tracing hepatocyte proliferation after PHx. (**B**) Whole-mount GFP fluorescence images of livers collected at different time points after PHx. (**C**) Immunostaining for GFP, GS, E-CAD, and β-catenin on liver sections collected at 24, 40, and 48 hours and 3, 4, and 7 days after PHx. Boxed regions are magnified in the right panel. (**D**) Quantification of the percentage of hepatocytes (Hep) expressing GFP in each zone of the liver lobule. Data are means ± SEM; $n = 5$. $^*P < 0.05$; ns, nonsignificant. Inset indicates the trend of GFP^+ hepatocyte percentage over time on the basis of quantification data. Scale bars: yellow, 1 mm; white, 100 μm. Each image is representative of five individual biological samples.

methods to assess proliferation, ProTracer could genetically segregate a rare signal of interest from the potentially much more intense background signals of other proliferating cells, thereby allowing the detection of specific patterning for restricted cell proliferation (Fig. 4A). Third, ProTracer using live imaging reporters (e.g., luciferase) permits noninvasive, long-term monitoring of cell proliferation in live animals (Fig. 4, K and L), which provides researchers with a temporally continuous tool for investigating cell proliferation dynamics in the same animal over windows of time ranging from hours to months or even longer. Fourth, ProTracer's readout can be a fluorescent signal, which enables the subsequent isolation and analysis of labeled cells, such as gene profiling, cell transplantation, and functional in vitro studies.

A key question in the field of liver biology pertains to the contribution of different hepatocyte populations to liver homeostasis and regeneration. Diverse findings have attributed increased proliferative capacity to different hepatocyte subpopulations (*12*–*17*, *24*). Although such studies have been dependent on a marker gene for lineage tracing or have followed a representative sample of all hepatocytes, ProTracer supports population-level analysis for all cells of a given type, as detailed in our work, and thus enables the unbiased detection of cellular compartments with proliferative capacity. In line with recent findings (*14*, *17*, *18*, *24*), our work argues against $Axin2^+$ pericentral hepatocytes being bona fide hepatic stem cells as previously proposed (*12*). Contrary to studies that suggest a broad contribution of hepatocytes in all zones to liver homeostasis (*14*, *16*, *18*), our ProTracer analysis suggests a population of hepatocytes located in zone 2 with more proliferative capacity during liver homeostasis, which creates the donut-like shape observed in our diverse proliferation-recording experiments. It is conceivable that other studies have not directly identified this zone because of lineage tracing of different hepatocyte populations or low labeling efficiency of their respective model. Related zonal hepatocyte proliferation analyses by EdU incorporation or Ki67 staining might have been too short to detect the population we observed (*14*, *18*). Likewise, ProTracer required continuous recording over several weeks to months to identify the zonal dominance of hepatocyte proliferation, likely because of the low turnover of hepatocytes during liver homeostasis (*18*). Notably, study of lineage tracing of a random sampling of hepatocytes in all zones (*24*) and EdU incorporation assays (*16*) have shown predominant proliferation in the midlobular zone of liver homeostasis.

Previous studies have suggested that a wave of hepatocyte proliferation from zone 1 toward zone 3 promotes regeneration in response to PHx (*18*, *48*–*52*). ProTracer confirms the portal-to-central regenerative wave and extends previous findings by providing higher-resolution and cumulative recording of the most proliferative events in hepatocytes during liver regeneration. Cumulative recording highlights that zone 2 contributes the most to liver regrowth during the peak proliferative response within the first 72 hours, whereas overall hepatocytes in zones 2 and 1 contributed equally to liver regrowth. By contrast, we found that hepatocytes in zone 3 contribute significantly less to liver regrowth, indicating that pericentral hepatocytes have limited liver stem cell potential. Additionally, we extend previous findings on the multicellular dynamics of liver regeneration (*55*) by showing the time windows of the proliferate waves of macrophages, cholangiocytes, hepatic stellate cells, and endothelial cells during liver regrowth from PHx. Future cell type–specific ProTracer experiments could provide additional resolution to this process. After some zonal injuries, ProTracer preferentially recorded zone 2 hepatocytes. Because most liver injuries occur in zones 1 or 3 (*56*), hepatocytes in zone 2 may be called into action more frequently as direct neighbors to both of these zones. It is therefore possible that the increased hepatocyte proliferation in zone 2, which we observed after CCl_4 or BDL injury, was at least in part induced by hepatocyte injury in neighboring zones. Similarly, it was demonstrated that liver regeneration is mainly mediated by the proliferation of hepatocytes next to the injured area and supported by auxiliary hepatocyte regeneration in other zones (*18*, *24*). The exact mechanisms conferring increased proliferative potential on zone 2 hepatocytes remain to be identified in the future. Our findings and the ProTracer model will enable future studies to further dissect the regenerative potential of diverse cell compartments in the liver and other organs.

Materials and methods summary

All mouse experiments were carried out in accordance with the current guidelines of the Institutional Animal Care and Use Committee (IACUC) at the Center for Excellence in Molecular Cell Science, Shanghai Institute of Biochemistry and Cell Biology, and the Institute for Nutritional Sciences, Shanghai Institute for Biological Sciences, Chinese Academy of Sciences. Mouse embryonic fibroblasts were isolated from E14.5 *Ki67-CrexER;R26-GFP* embryos for live cell imaging, and aortas were dissociated from *Ki67-CrexER;R26-GFP* mice aged 8 to 9 weeks to visualize the proliferated aortic endothelial cells. These experiments were performed to examine the utility of the *Ki67-CrexER* allele as a representative marker of cell proliferation. Protracer was primed by Tam or AAV-Dre induction for the initiation of genetic recording of cell proliferation. The sparse labeling of proliferated hepatocytes was performed by induction of a low dose of AAV or Tam on ProTracer mice. This experiment was performed to test whether most of the Protracer-labeled hepatocytes had undergone cell division. Liver injury models that include CCl_4 injury, PHx, and BDL were performed on ProTracer mice at 1 to 7 days after Tam induction to study hepatocyte proliferation during liver repair and regeneration. Information regarding the AAV virus production, whole-mount fluorescence microscopy, tissue immunostaining, bioluminescence imaging, Southern blot analysis, liver clearing, and light-sheet microscopy are provided in detail in the supplementary materials.

REFERENCES AND NOTES

1. G. K. Michalopoulos, M. C. DeFrances, Liver regeneration. *Science* **276**, 60–66 (1997). doi: 10.1126/science.276.5309.60; pmid: 9082986
2. C. Blanpain, B. D. Simons, Unravelling stem cell dynamics by lineage tracing. *Nat. Rev. Mol. Cell Biol.* **14**, 489–502 (2013). doi: 10.1038/nrm3625; pmid: 23860235
3. A. Miyajima, M. Tanaka, T. Itoh, Stem/progenitor cells in liver development, homeostasis, regeneration, and reprogramming. *Cell Stem Cell* **14**, 561–574 (2014). doi: 10.1016/j.stem.2014.04.010; pmid: 24792114
4. A. J. Merrell, B. Z. Stanger, Adult cell plasticity *in vivo*: De-differentiation and transdifferentiation are back in style. *Nat. Rev. Mol. Cell Biol.* **17**, 413–425 (2016). doi: 10.1038/nrm.2016.24; pmid: 26979497
5. C. L. Cai *et al.*, A myocardial lineage derives from *Tbx18* epicardial cells. *Nature* **454**, 104–108 (2008). doi: 10.1038/nature06969; pmid: 18480752
6. B. Beck *et al.*, A vascular niche and a VEGF-Nrp1 loop regulate the initiation and stemness of skin tumours. *Nature* **478**, 399–403 (2011). doi: 10.1038/nature10525; pmid: 22012397
7. A. Van Keymeulen *et al.*, Distinct stem cells contribute to mammary gland development and maintenance. *Nature* **479**, 189–193 (2011). doi: 10.1038/nature10573; pmid: 21983963
8. J. C. Larsimont *et al.*, Sox9 Controls Self-Renewal of Oncogene Targeted Cells and Links Tumor Initiation and Invasion. *Cell Stem Cell* **17**, 60–73 (2015). doi: 10.1016/j.stem.2015.05.008; pmid: 26095047

9. G. Zajicek, R. Oren, M. Weinreb Jr., The streaming liver. *Liver* **5**, 293–300 (1985). doi: 10.1111/j.1600-0676.1985.tb00252.x; pmid: 4088003
10. M. P. Bralet, S. Branchereau, C. Brechot, N. Ferry, Cell lineage study in the liver using retroviral mediated gene transfer. Evidence against the streaming of hepatocytes in normal liver. *Am. J. Pathol.* **144**, 896–905 (1994). pmid: 8178942
11. G. Zajicek, Do livers "stream"? *Am. J. Pathol.* **146**, 772–776 (1995). pmid: 7887457
12. B. Wang, L. Zhao, M. Fish, C. Y. Logan, R. Nusse, Self-renewing diploid Axin2$^+$ cells fuel homeostatic renewal of the liver. *Nature* **524**, 180–185 (2015). doi: 10.1038/nature14863; pmid: 26245375
13. J. Font-Burgada *et al*., Hybrid Periportal Hepatocytes Regenerate the Injured Liver without Giving Rise to Cancer. *Cell* **162**, 766–779 (2015). doi: 10.1016/j.cell.2015.07.026; pmid: 26276631
14. L. Planas-Paz *et al*., The RSPO-LGR4/5-ZNRF3/RNF43 module controls liver zonation and size. *Nat. Cell Biol.* **18**, 467–479 (2016). doi: 10.1038/ncb3337; pmid: 27088858
15. W. Pu *et al*., Mfsd2a$^+$ hepatocytes repopulate the liver during injury and regeneration. *Nat. Commun.* **7**, 13369 (2016). doi: 10.1038/ncomms13369; pmid: 27857132
16. S. Lin *et al*., Distributed hepatocytes expressing telomerase repopulate the liver in homeostasis and injury. *Nature* **556**, 244–248 (2018). doi: 10.1038/s41586-018-0004-7; pmid: 29618815
17. C. H. Ang *et al*., Lgr5$^+$ pericentral hepatocytes are self-maintained in normal liver regeneration and susceptible to hepatocarcinogenesis. *Proc. Natl. Acad. Sci. U.S.A.* **116**, 19530–19540 (2019). doi: 10.1073/pnas.1908099116; pmid: 31488716
18. T. Sun *et al*., AXIN2$^+$ Pericentral Hepatocytes Have Limited Contributions to Liver Homeostasis and Regeneration. *Cell Stem Cell* **26**, 97–107.e6 (2020). doi: 10.1016/j.stem.2019.10.011; pmid: 31866224
19. A. Raven *et al*., Cholangiocytes act as facultative liver stem cells during impaired hepatocyte regeneration. *Nature* **547**, 350–354 (2017). doi: 10.1038/nature23015; pmid: 28700576
20. X. Deng *et al*., Chronic Liver Injury Induces Conversion of Biliary Epithelial Cells into Hepatocytes. *Cell Stem Cell* **23**, 114–122.e3 (2018). doi: 10.1016/j.stem.2018.05.022; pmid: 29937200
21. S. Shin, N. Upadhyay, L. E. Greenbaum, K. H. Kaestner, Ablation of *Foxl1-Cre*-labeled hepatic progenitor cells and their descendants impairs recovery of mice from liver injury. *Gastroenterology* **148**, 192–202.e3 (2015). doi: 10.1053/j.gastro.2014.09.039; pmid: 25286440
22. J. O. Russell *et al*., Hepatocyte-Specific β-Catenin Deletion During Severe Liver Injury Provokes Cholangiocytes to Differentiate Into Hepatocytes. *Hepatology* **69**, 742–759 (2019). doi: 10.1002/hep.30270; pmid: 30215850
23. T. Matsumoto, L. Wakefield, B. D. Tarlow, M. Grompe, In Vivo Lineage Tracing of Polyploid Hepatocytes Reveals Extensive Proliferation during Liver Regeneration. *Cell Stem Cell* **26**, 34–47.e3 (2020). doi: 10.1016/j.stem.2019.11.014; pmid: 31866222
24. F. Chen *et al*., Broad Distribution of Hepatocyte Proliferation in Liver Homeostasis and Regeneration. *Cell Stem Cell* **26**, 27–33.e4 (2020). doi: 10.1016/j.stem.2019.11.001; pmid: 31866223
25. K. Kretzschmar *et al*., Profiling proliferative cells and their progeny in damaged murine hearts. *Proc. Natl. Acad. Sci. U.S.A.* **115**, E12245–E12254 (2018). doi: 10.1073/pnas.1805829115; pmid: 30530645
26. O. Basak *et al*., Troy+ brain stem cells cycle through quiescence and regulate their number by sensing niche occupancy. *Proc. Natl. Acad. Sci. U.S.A.* **115**, E610–E619 (2018). doi: 10.1073/pnas.1715911114; pmid: 29311336
27. S. P. Robinson, S. M. Langan-Fahey, D. A. Johnson, V. C. Jordan, Metabolites, pharmacodynamics, and pharmacokinetics of tamoxifen in rats and mice compared to the breast cancer patient. *Drug Metab. Dispos.* **19**, 36–43 (1991). pmid: 1673419
28. G. Yang, S. Nowsheen, K. Aziz, A. G. Georgakilas, Toxicity and adverse effects of Tamoxifen and other anti-estrogen drugs. *Pharmacol. Ther.* **139**, 392–404 (2013). doi: 10.1016/j.pharmthera.2013.05.005; pmid: 23711794
29. Y. Li *et al*., Genetic Lineage Tracing of Nonmyocyte Population by Dual Recombinases. *Circulation* **138**, 793–805 (2018). doi: 10.1161/CIRCULATIONAHA.118.034250; pmid: 29700121
30. H. Zhang *et al*., Endocardium Contributes to Cardiac Fat. *Circ. Res.* **118**, 254–265 (2016). doi: 10.1161/CIRCRESAHA.115.307202; pmid: 26659641
31. W. Pu *et al*., Genetic Targeting of Organ-Specific Blood Vessels. *Circ. Res.* **123**, 86–99 (2018). doi: 10.1161/CIRCRESAHA.118.312981; pmid: 29764841
32. K. B. Halpern *et al*., Single-cell spatial reconstruction reveals global division of labour in the mammalian liver. *Nature* **542**, 352–356 (2017). doi: 10.1038/nature21065; pmid: 28166538
33. K. Jungermann, T. Keitzmann, Zonation of parenchymal and nonparenchymal metabolism in liver. *Annu. Rev. Nutr.* **16**, 179–203 (1996). doi: 10.1146/annurev.nu.16.070196.001143; pmid: 8839925
34. S. Colnot, C. Perret, in *Liver Zonation*, S. P. S. Monga, Ed. (Springer, 2011), pp. 7–16.
35. N. Aizarani *et al*., A human liver cell atlas reveals heterogeneity and epithelial progenitors. *Nature* **572**, 199–204 (2019). doi: 10.1038/s41586-019-1373-2; pmid: 31292543
36. H. Zhang *et al*., Endocardium Minimally Contributes to Coronary Endothelium in the Embryonic Ventricular Free Walls. *Circ. Res.* **118**, 1880–1893 (2016). doi: 10.1161/CIRCRESAHA.116.308749; pmid: 27056912
37. K. Yanger *et al*., Adult hepatocytes are generated by self-duplication rather than stem cell differentiation. *Cell Stem Cell* **15**, 340–349 (2014). doi: 10.1016/j.stem.2014.06.003; pmid: 25130492
38. B. D. Tarlow *et al*., Bipotential adult liver progenitors are derived from chronically injured mature hepatocytes. *Cell Stem Cell* **15**, 605–618 (2014). doi: 10.1016/j.stem.2014.09.008; pmid: 25312494
39. J. R. Schaub, Y. Malato, C. Gormond, H. Willenbring, Evidence against a stem cell origin of new hepatocytes in a common mouse model of chronic liver injury. *Cell Rep.* **8**, 933–939 (2014). doi: 10.1016/j.celrep.2014.07.003; pmid: 25131204
40. R. Manco *et al*., Reactive cholangiocytes differentiate into proliferative hepatocytes with efficient DNA repair in mice with chronic liver injury. *J. Hepatol.* **70**, 1180–1191 (2019). doi: 10.1016/j.jhep.2019.02.003; pmid: 30794890
41. Y. Wang *et al*., Genetic tracing of hepatocytes in liver homeostasis, injury, and regeneration. *J. Biol. Chem.* **292**, 8594–8604 (2017). doi: 10.1074/jbc.M117.782029; pmid: 28377509
42. L. Madisen *et al*., Transgenic mice for intersectional targeting of neural sensors and effectors with high specificity and performance. *Neuron* **85**, 942–958 (2015). doi: 10.1016/j.neuron.2015.02.022; pmid: 25741722
43. G. Margall-Ducos, S. Celton-Morizur, D. Couton, O. Brégerie, C. Desdouets, Liver tetraploidization is controlled by a new process of incomplete cytokinesis. *J. Cell Sci.* **120**, 3633–3639 (2007). doi: 10.1242/jcs.016907; pmid: 17895361
44. Y. Miyaoka *et al*., Hypertrophy and unconventional cell division of hepatocytes underlie liver regeneration. *Curr. Biol.* **22**, 1166–1175 (2012). doi: 10.1016/j.cub.2012.05.016; pmid: 22658593
45. T. Katsuda *et al*., Transcriptomic Dissection of Hepatocyte Heterogeneity: Linking Ploidy, Zonation, and Stem/Progenitor Cell Characteristics. *Cell. Mol. Gastroenterol. Hepatol.* **9**, 161–183 (2020). doi: 10.1016/j.jcmgh.2019.08.011; pmid: 31493546
46. M. Hirai, J. Chen, S. M. Evans, Tissue-Specific Cell Cycle Indicator Reveals Unexpected Findings for Cardiac Myocyte Proliferation. *Circ. Res.* **118**, 20–28 (2016). doi: 10.1161/CIRCRESAHA.115.307697; pmid: 26472817
47. C. Mitchell, H. Willenbring, A reproducible and well-tolerated method for 2/3 partial hepatectomy in mice. *Nat. Protoc.* **3**, 1167–1170 (2008). doi: 10.1038/nprot.2008.80; pmid: 18600221
48. J. W. Grisham, A morphologic study of deoxyribonucleic acid synthesis and cell proliferation in regenerating rat liver; autoradiography with thymidine-H3. *Cancer Res.* **22**, 842–849 (1962). pmid: 13902009
49. H. M. Rabes, in *Ciba Foundation Symposium 55 - Hepatotrophic Factors*, R. Porter, J. Whelan, Eds. (Novartis Foundation Symposia, Wiley, 1978), 31–53.
50. R. L. Jirtle, B. I. Carr, C. D. Scott, Modulation of insulin-like growth factor-II/mannose 6-phosphate receptors and transforming growth factor-β1 during liver regeneration. *J. Biol. Chem.* **266**, 22444–22450 (1991). doi: 10.1016/S0021-9258(18)54592-0; pmid: 1718994
51. T. H. Kim, W. M. Mars, D. B. Stolz, G. K. Michalopoulos, Expression and activation of pro-MMP-2 and pro-MMP-9 during rat liver regeneration. *Hepatology* **31**, 75–82 (2000). doi: 10.1002/hep.510310114; pmid: 10613731
52. M. Preziosi, H. Okabe, M. Poddar, S. Singh, S. P. Monga, Endothelial Wnts regulate β-catenin signaling in murine liver zonation and regeneration: A sequel to the Wnt-Wnt situation. *Hepatol. Commun.* **2**, 845–860 (2018). doi: 10.1002/hep4.1196; pmid: 30027142
53. B. Lehner *et al*., The dark side of BrdU in neural stem cell biology: Detrimental effects on cell cycle, differentiation and survival. *Cell Tissue Res.* **345**, 313–328 (2011). doi: 10.1007/s00441-011-1213-7; pmid: 21837406
54. L. H. Levkoff *et al*., Bromodeoxyuridine inhibits cancer cell proliferation *in vitro* and *in vivo*. *Neoplasia* **10**, 804–816 (2008). doi: 10.1593/neo.08382; pmid: 18680882
55. G. K. Michalopoulos, Hepatostat: Liver regeneration and normal liver tissue maintenance. *Hepatology* **65**, 1384–1392 (2017). doi: 10.1002/hep.28988; pmid: 27997988
56. S. J. Forbes, P. N. Newsome, Liver regeneration - mechanisms and models to clinical application. *Nat. Rev. Gastroenterol. Hepatol.* **13**, 473–485 (2016). doi: 10.1038/nrgastro.2016.97; pmid: 27353402

ACKNOWLEDGMENTS

We thank the Shanghai Model Organisms Center, Inc. (SMOC) for mouse generation; institutional animal facilities for mice husbandry; and H. Zeng for providing reporter mice. We also acknowledge technical help from W. Bian, J. Tang, and members of the National Center for Protein Science Shanghai for assistance in microscopy. We thank J. H. Snyder for editing the manuscript. **Funding:** This work was supported by the Strategic Priority Research Program of the Chinese Academy of Sciences (CAS; XDB19000000 and XDA16010507), the National Key Research & Development Program of China (2019YFA0110403, 2018YFA0107900, 2019YFA0110400, 2018YFA0108100, and 2017YFC1001303), the National Science Foundation of China (82088101, 31730112, 31625019, 91849202, 32050087, 91639302, 81872241, and 31922032), the Youth Innovation Promotion Association of CAS, the Key Project of Frontier Sciences of CAS (QYZDB-SSW-SMC003), the innovative research teams of high-level local universities in Shanghai, the Shanghai Science and Technology Commission (19JC1415700 and 19ZR1479800), the Program for Guangdong Introduction Innovative and Entrepreneurial Teams (2017ZT07S347), the Shanghai Rising-Star Project, the China Postdoctoral Science Foundation, the China Postdoctoral Innovative Talent Support Program, the SIBS President Fund, the Royal Society-Newton Advanced Fellowship, AstraZeneca, and the support from the XPLORER PRIZE. **Author contributions:** L.H., W.P., and X.L. designed the study, performed experiments, and analyzed the data. Z.Z., M.H., Yi L., X.Hu., X.Ha., Ya.L., K.L., M.S., Q.-D.W., and Y.J. bred the mice, performed experiments, or provided intellectual input. L.L. and R.S. performed Southern blotting and generated mice. J.S.T. provided intellectual input and edited the manuscript. B.Z. conceived and supervised the study and wrote the manuscript. **Competing interests:** The authors have no competing interests. **Data and materials availability:** All data are available in the manuscript or the supplementary materials. Materials will be provided on reasonable request. ProTracer mice and their related plasmids will be deposited at commercial animal companies and Addgene, respectively, where they will be publicly available.

SUPPLEMENTARY MATERIALS

science.sciencemag.org/content/371/6532/eabc4346/suppl/DC1
Materials and Methods
Figs. S1 to S16
References (57–64)
MDAR Reproducibility Checklist
Movie S1

View/request a protocol for this paper from *Bio-protocol*.

21 May 2020; accepted 30 November 2020
10.1126/science.abc4346

Science

Proliferation tracing reveals regional hepatocyte generation in liver homeostasis and repair

Lingjuan He, Wenjuan Pu, Xiuxiu Liu, Zhenqian Zhang, Maoying Han, Yi Li, Xiuzhen Huang, Ximeng Han, Yan Li, Kuo Liu, Mengyang Shi, Liang Lai, Ruilin Sun, Qing-Dong Wang, Yong Ji, Jan S. Tchorz and Bin Zhou

Science **371** (6532), eabc4346.
DOI: 10.1126/science.abc4346

Zoning in on liver growth

For organ homeostasis or regrowth after injury or disease, one or more stem cell populations is needed to rebuild lost tissue. There is considerable debate about the source of new cells in the liver. Two groups now identify the source of new hepatocytes (see the Perspective by Andersson). Although the liver may seem to lack major variation across its structure, its lobule is organized into concentric zones where hepatocytes express different metabolic enzymes. Wei *et al.* sought to systematically define the source of new liver cells by comparing 14 fate-mapping mice that label different liver cell types. They found that different regions of the liver lobule exhibit differences in hepatocyte turnover, with zone 2 representing a primary source of new hepatocytes during homeostasis and regeneration. Similarly, He *et al.* designed a genetic approach to record cell proliferation in vivo with high spatial and temporal resolution to enable continuous recording of proliferative events of any specific cell type at the whole-cell population level. Using this method, they identified zone 2 as having the highest proliferative activity and contributing the most to liver regrowth. These findings have implications for the cellular basis of chronic disease pathogenesis, cancer development, and regenerative medicine strategies.

Science, this issue p. eabb1625, p. eabc4346; see also p. 887

Science (print ISSN 0036-8075; online ISSN 1095-9203) is published by the American Association for the Advancement of Science, 1200 New York Avenue NW, Washington, DC 20005. The title *Science* is a registered trademark of AAAS.